Topographic and Morphologic Analyses of Retinal Ganglion Cell Loss in Old DBA/2NNia Mice

Theodoros Filippopoulos,[1,2] *John Danias,*[2] *Bin Chen,*[2] *Steven M. Podos,*[2,3] *and Thomas W. Mittag*[2]

Purpose. To evaluate the relationship between retinal ganglion cell (RGC) size, density distribution, and survival in senescent DBA2/NNia mice that develop pigmentary glaucoma. To evaluate the validity of nearest neighbor distance (NND), a measure of focal density for surviving RGCs in the retina, as a method to quantify RGC loss in mice.

Methods. Fifteen-month-old DBA2/NNia mice were labeled retrogradely with fluorogold. Retinas were flat mounted and imaged in their entirety using an epifluorescence microscope with a motorized stage. Digital maps of the retinal whole-mounts were constructed to automatically count and establish spatial coordinates for RGCs over the entire retina. RGC size and NND were determined from these maps.

Results. RGC counts in the group of 15-month-old DBA/2NNia animals ranged from 22,330 to 92,157 cells per retina. Mean RGC cell size per retina ranged from 22.35 to 35.64 μm^2 and correlated linearly with total RGC counts. NND distribution histograms were compared for retinas with variable degrees of RGC loss. The distribution of NNDs in each retina was skewed toward larger distance values in more affected retinas. In partially damaged retinas, areas with severe pathology coincided with areas of maximal loss of large RGCs, and areas of preserved RGCs correlated with larger cell sizes.

Conclusions. Damaged retinas have a smaller mean cell size, indicating preferential loss of larger RGCs or size reduction of surviving cells. NND analysis of the RGC population in a retina is a useful measure of glaucomatous RGC loss. The skewed NND distribution of surviving RGCs and the finding that RGC loss correlates with a shift/amplitude change in the mode of the histogram and its tail suggests two different patterns of RGC loss possibly attributable to different pathologic processes in glaucomatous DBA/2 mice. (*Invest Ophthalmol Vis Sci.* 2006;47:1968–1974) DOI:10.1167/iovs.05-0955

Induced glaucoma models in the rat have been the subject of increasing research interest in recent years[1–5] and have been used to evaluate substances with potential neuroprotective or antiapoptotic properties.[6–10] These models exhibit a range of pathology, most likely because of the diverse characteristics and the severity and duration of the surgical insult used to induce IOP elevation.

More recently, murine models of glaucomatous optic neuropathy have also become of interest to some investigators.[11–16] Highly inbred mouse strains have a more restricted biologic variability that, together with spontaneous or gene-induced development of high IOP,[11,12,17–19] makes them desirable glaucoma models for investigation. Other potentially important examples for glaucoma research are mice with gene knockouts of components of the apoptotic cell death program of neurons,[20,21] which is thought to be the primary mechanism for retinal ganglion cell (RGC) loss in glaucoma. A critical requirement in most studies of mouse glaucoma models is the quantification of RGC somata or their axons.

Automated counting methods to quantify RGC loss in the glaucomatous retina have certain advantages over manual counting based on sampling.[22] The assessment of RGCs in virtually 100% of the retinal area provides increased counting precision and allows the investigation of spatial and cell size patterns of surviving RGCs in a retina with glaucoma. In this study, we examined the detailed spatial arrangement and the cell size of RGCs in murine retinas with different degrees of glaucomatous RGC loss. We used an automated counting method to quantify the glaucomatous focal RGC loss encountered in aged DBA/2NNia mice.[16] The spontaneous development of secondary glaucoma in this mouse strain is partially age and sex dependent and results from gene mutations causing iris atrophy and pigment dispersion,[12] together with an immunologic component,[23] that is not yet fully understood. Therefore, individual eyes in a nonselected, mixed-sex population of DBA/2 mice of the same age can exhibit a range of retinal pathology. We used such a group of mice at 15 months of age to study the patterns of RGC survival in retinas with varying degrees of glaucomatous neuropathy. We created data libraries of the studied retinas and digitally constructed spatial RGC maps to extend the analysis from cell counts to morphologic and topographic associations of surviving RGCs. To further characterize the previously reported spatial non-uniformity of RGC loss,[16] we investigated the use of nearest neighbor distance (NND) for every RGC in a retina as a measure of focal RGC density. NND is defined as the distance between the centroid of each RGC and the centroid of its closest neighbor. The centroid is defined as the moment center for each object and can be calculated for any object, symmetric or asymmetric. It corresponds to its geometric center for a symmetric object. NND and the spatial coordinates of the centroid for each object in a binary image are directly provided by a plug-in of Photoshop 5.5 (Adobe, San Jose, CA).[24] Consequently, for each cell, the NND approximates the radius of a circular retinal area occupied by that cell alone. NND is thus inversely related to RGC density and is independent of the constraints inherent in density analysis of RGCs calculated from sampling frames. Therefore, the NND approach has potential advantages for quantifying and characterizing the overall RGC loss in a retina compared with gross RGC counts estimated from sampling or frame cell density analysis.

From the [1]Department of Ophthalmology, Brown University Medical School, Providence, Rhode Island; and the Departments of [2]Ophthalmology and [3]Neuroscience, Mount Sinai School of Medicine, New York, New York.

Supported by the Kriezis Foundation; National Institutes of Health Grants R01 EY13399, NEI K08 00390, R01 EY015224, EY13467, EY01867; Research to Prevent Blindness; and the Fund for Ophthalmic Knowledge.

Submitted for publication July 22, 2005; revised November 19, 2005; accepted March 13, 2006.

Disclosure: **T. Filippopoulos**, None; **J. Danias**, None; **B. Chen**, None; **S.M. Podos**, None; **T.W. Mittag**, None

The publication costs of this article were defrayed in part by page charge payment. This article must therefore be marked "*advertisement*" in accordance with 18 U.S.C. §1734 solely to indicate this fact.

Corresponding author: Theodoros Filippopoulos, Department of Ophthalmology, Brown University Medical School, APC 7th, 593 Eddy Street, Providence, RI 02903; theodoros_filippopoulos@brown.edu.

METHODS

All animals were handled in accordance with the ARVO Statement for the Use of Animals in Ophthalmic and Vision Research. A group of 15-month-old DBA/2NNia[11,16,25] mice ($n = 5$ animals, mixed sex) was used for this experiment. Animals had been housed in covered cages, fed with a standard rodent diet ad libitum, and kept under constant 12-hour light/12-hour dark cycles.

Retrograde Labeling

Mice were anesthetized by intraperitoneal administration of xylazine (10.8 mg/kg), acepromazine (1.2 mg/kg), and ketamine (54.0 mg/kg). Their skulls were exposed, and holes 2 mm in diameter were drilled bilaterally at points 2.92 mm posterior and 0.5 mm lateral to the bregma to expose the occipital cortex.[26,27] Under constant direct observation, the occipital cortex overlying the superior colliculus (SC) was gently aspirated and the SC was exposed. A piece of gel foam (Pharmacia & Upjohn, Kalamazoo, MI) soaked in 5% aqueous fluorogold (Fluorochrome, Denver, CO) was applied to each SC. The gel foam was covered with antibiotic ointment, and the overlying skin was sutured.

Flat Mounting/Digital Imaging

After 7 days, to allow for the retrograde labeling of retinal ganglion cells, the animals were humanely killed by transcardial perfusion with 4% paraformaldehyde in 0.1 M phosphate-buffered saline under general anesthesia. Eyes were immediately enucleated; retinas were dissected from the globes and prepared as flattened wholemounts after relaxing incisions were performed, preserving orientation. Retinal wholemounts were imaged on an epifluorescence microscope (Axioskop 2; Zeiss, Thornwood, NY) equipped with a digital camera (Monospot; Diagnostic Instrumentation Inc., Sterling Heights, MI) and a motorized stage (Biopoint; Ludl Electronic Products, Ltd., Hawthorne, NY), allowing the sequential acquisition of adjacent nonoverlapping frames that covered the total area of each retina.[22] Imaging was performed with a 10× objective, NA 0.50 mm (Zeiss), in 30 frames per retina arranged in a reproducible 5 × 6 grid. Images from 8 of 10 flat-mounted retinas of adequate quality were further analyzed for construction of NND maps.

Digital Processing

Commercially available software (Photoshop 5.5 [Adobe]; Image Tool 2.0 [University of Texas Health Science Center at San Antonio, San Antonio, TX]) was used to convert the fluorescent digital retinal images to corresponding black-and-white images used for the subsequent analysis, as previously described.[16,22]

To validate the automated RGC counting method for this imaging setup, automated counts were compared with those obtained from images counted manually by two investigators in a masked fashion. More than 146,000 manually counted RGCs from another set of flat-mounted retinal images were used for this purpose. The size threshold criteria for black objects representing RGCs versus background were determined by calculating the object size in pixels of the smallest among a large number of RGCs positively identified on the original images as RGCs. This size threshold coincided with the inflection point of the object size distribution in the set of manually counted frames, as previously reported.[16,22] This inflection point separated the bimodal object size distribution, with the first mode representing the noise and the latter representing RGCs. In addition, the determined size threshold provided the highest correlation between manual and automated counts ($R^2 = 0.9631$) (Fig. 1). By using this algorithm, total RGC counts were determined for the eight retinas studied in detail.

Data Analysis

Digital data libraries were created for each retina; every counted object was represented by its position coordinates and contained information on object size, object symmetry, and relationship to adjacent objects.

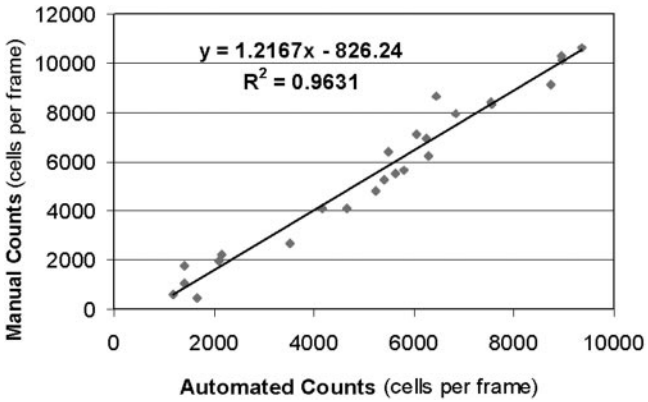

FIGURE 1. Validation of counting algorithm for the imaging set-up described in Methods. Manual Counts = f (Automated Counts) in cells per frame (linear correlation $R^2 = 0.9631$ [$P < 0.001$] for the regression coefficient).

Software (Photoshop 5.5; Adobe) was used to record the spatial coordinates of the moment center (centroid) of each object in the converted black-and-white binary images that represented the RGCs imaged on the epifluorescence microscope,[16,22] along with other information such as equivalent cell diameter and symmetry (function: measure all in Photoshop 5.5; Adobe). One of these measures is NND, defined as centroid-to-centroid distance of one object to its closest neighbor.[24] We also constructed retinal NND maps of all eight retinas studied by plotting the spatial coordinates of each object (RGC) and its corresponding NND value in statistical analysis software (NCSS, Kaysville, UT).

Finally, from the same data libraries, we calculated a mean object size, reflected by its area, for all objects (RGCs) and correlated this value with the total RGC counts. Pixel size for an object was converted (Photoshop 5.5; Adobe) to a circular area of equivalent diameter providing, in this case, an estimate of RGC size (function: measure all in Photoshop 5.5; Adobe).

Statistical Analysis

Commercial programs (NCSS 2000 and PASS 6.0 [NCSS]; Excel 2000 [Microsoft Corp., Redmond, WA]) were used to perform all statistical analyses.

RESULTS

Total RGC Counts

The eight retinas of the 15-month-old DBA/2NNia mice showed a great degree of variability in pathology, with total counts of surviving RGCs ranging between 22,330 and 92,157 cells. The mean (± SD) count for the group was 49,849.5 ± 27,397 cells. There was no statistically significant difference between right and left eyes: 50,173.6 ± 24,688.8 and 49,399.1 ± 37,463.7 cells, respectively ($P = 0.97$; Student t test). The average retinal area for the group was 20 ± 1.3 mm^2, and the average cell density was 2497 ± 1388 RGCs/mm^2. However, these numerical values do not illustrate the wide range of RGC loss encountered in this group of 15-month-old DBA2/NNia retinas.

Nearest Neighbor Distance

Mean NND values correlated well with total cell counts for all retinas ($R^2 = 0.9621$; 95% confidence interval, 0.971–0.987; $P < 0.001$) (Fig. 2).

To further evaluate the relationship between cell loss and NND, retinas were subdivided into preserved and affected retinas according to total RGC number, and normalized NND histograms were created for the two groups. The NND distri-

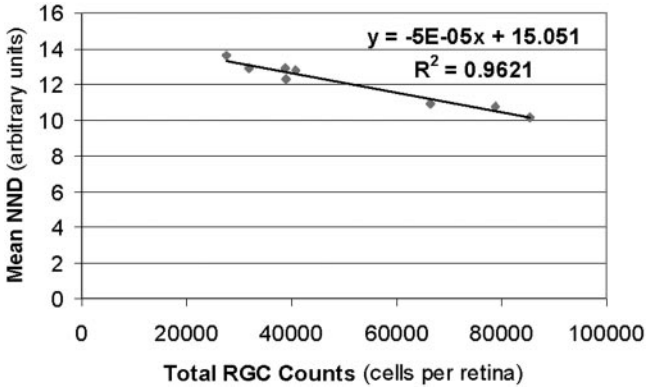

FIGURE 2. Mean NND per retina correlates linearly with total RGC count per retina. As RGC counts decrease, NNDs increase (1 arbitrary distance unit = 1.04 μm) (linear regression $R^2 = 0.9621$ [$P < 0.001$] for the regression coefficient).

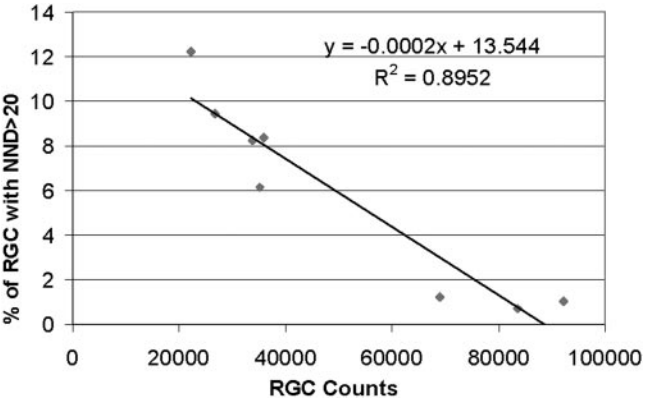

FIGURE 4. Linear correlation between percentage of cells with NNDs exceeding 20 arbitrary units and total RGC counts (linear regression $R^2 = 0.8958$ [$P < 0.001$] for the regression coefficient)

bution curve for all the RGCs in preserved retinas sorted into 42 bins is slightly skewed (asymmetric) and has a long tail representing the few cells (~1%-2%) with high NND values (Fig. 3A). Therefore, all objects whose NNDs exceeded 20 arbitrary units or 21.09 μm were included in the last bin for illustration purposes (Fig. 3A, histogram; Fig. 3B, cumulative plot). This percentage of cells with NND greater than 20 arbitrary units differed significantly between preserved retinas that maintained approximately 75% of their RGCs[16] (total RGCs > 64,000; $n = 3$) and severely affected retinas (total RGCs < 64,000; $n = 5$) ($P < 0.001$; Student t test) and was inversely related to the total count of surviving RGCs in senescent DBA/2NNia murine retinas, as shown in Figure 4 ($R^2 = 0.8958$).

Cells included in the right part of the histogram (Fig. 3A) with NNDs exceeding 20 arbitrary units were those surviving in areas of focal loss with few adjacent cells, as can be seen by inspection of the empty spaces in the NND retinal maps (Fig. 5). For NNDs less than 20 arbitrary units, the NND distribution for retinas with little or no RGC loss (RGCs > 64,000) was nearly symmetric. In comparison, retinas with decreased RGC counts showed a significant shift in the NND distribution curve toward higher NND values in this part of the histogram (Fig. 3A). This shift represented a diffuse type of RGC loss with wider spacing between RGCs, which were spatially more evenly distributed throughout the entire retinal RGC population, as better shown by the cumulative plot of the same data (Fig. 3B). This more diffuse type of RGC loss cannot be discerned when NND distribution was spatially mapped using only a few bins, as in Figure 5, which shows the NND maps of the studied retinas. For clarity the NND distribution bins in such maps was limited to a few color codes, in this case four.

RGC Cell Size

The mean cell size calculated from objects defined as RGCs by the counting parameters in the binary black-and-white images in the group of 15-month-old DBA/2NNia animals also showed a great degree of variability. Regression analysis gave a good linear correlation ($R^2 = 0.8751$; $P < 0.001$) between mean cell size per retina and total RGC count for that retina. On average, better preserved retinas had larger retinal ganglion cells (Fig. 6).

The size distribution of surviving RGCs (diameter of circular area equivalent to the pixel size of objects in the binary images) in retinas with significant cell loss showed that smaller RGCs are proportionately better preserved, thus causing a shift to the left of the normalized size distribution histogram (Fig. 7). Therefore, we can conclude that affected retinas include a smaller proportion of larger cells than do unaffected retinas.

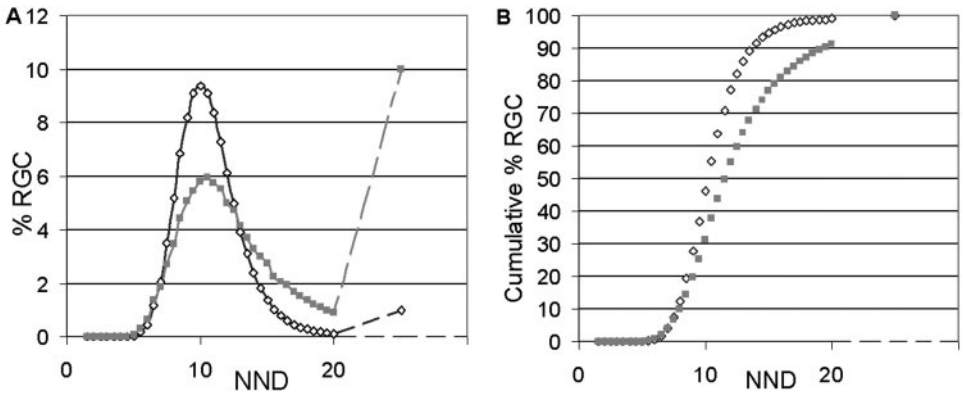

FIGURE 3. Normalized NND distribution in preserved and affected retinas. NND values for all RGCs in the most preserved retinas with RGC counts exceeding 64,000 ($n = 3$) and the most affected retinas with RGC counts less than 64,000 ($n = 5$) have been grouped together. (**A**) Large increase (almost ninefold) in the percentage of RGCs with NND greater than 20 in retinas with severe RGC loss. (**B**) Cumulative graph demonstrates the rightward shift of the NND distribution in the affected retinas, indicating a more uniform dropout of RGC over the retinal area. *Open symbols* represent the preserved retinas, and *closed symbols* represent the affected retinas.

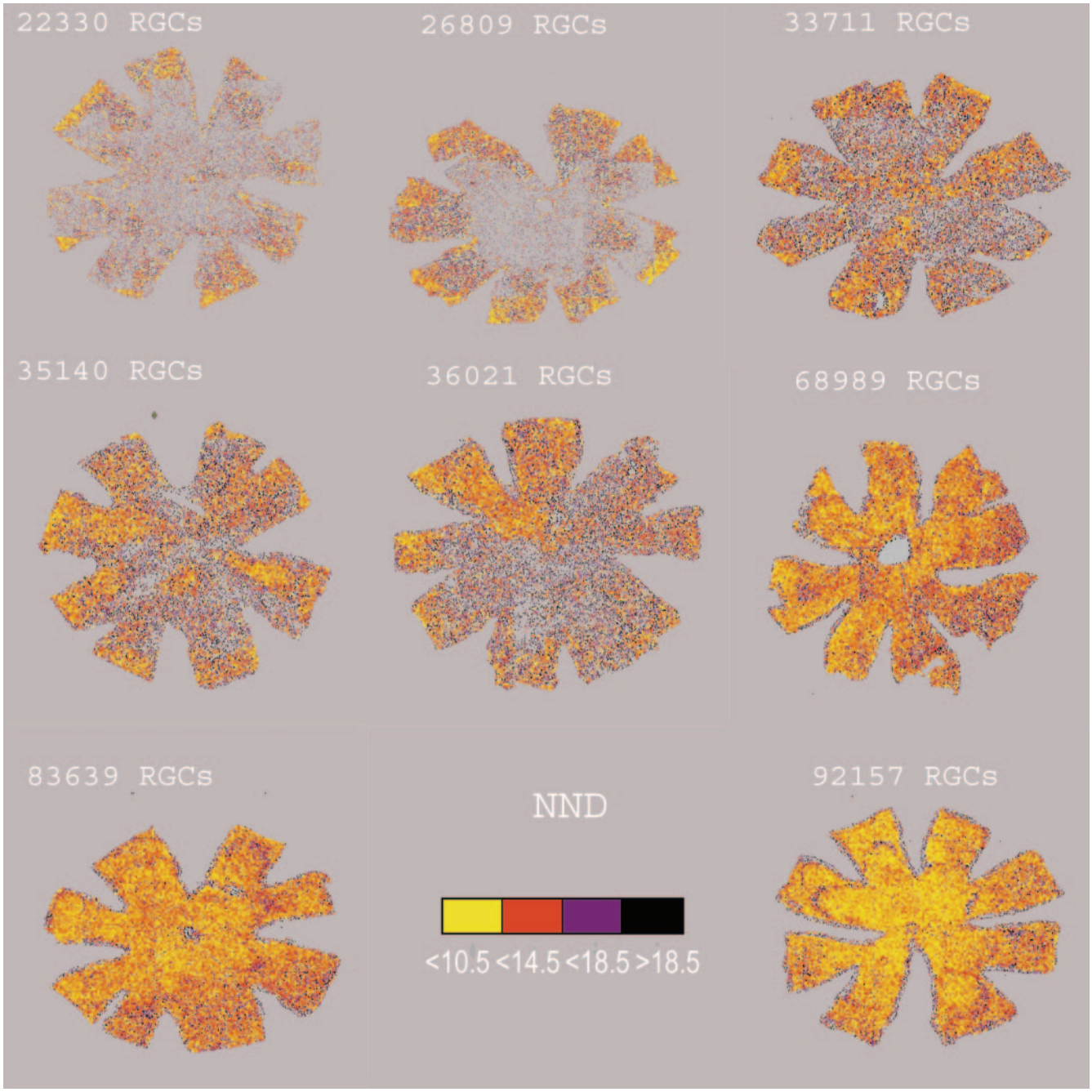

FIGURE 5. NND Maps for eight retinas from senescent DBA/2NNia mice. Each RGC, plotted at its spatial coordinates in the retina, is assigned a color code according to its NND value (color bar), with *yellow* indicating RGCs in high cell density (low NND) areas and *black* indicating those in lowest density areas. The color bar also indicates the bin distance range, in micrometers, used for constructing the color-coded maps. Note preservation of RGCs at the periphery of damaged retinas compared to mid central areas.

This preferential loss of larger RGCs in damaged areas could also be seen within a single retina. Figure 8 shows a retina with significant RGC loss but with large patches of preserved cells, as indicated by the NND map (left). The cell size map of the same retina (right) shows that increased RGC size was spatially correlated to the areas of RGC preservation (indicated by the smaller NNDs of cells in the map on the left).

DISCUSSION

Aged DBA/2NNia mice can show considerable variability with respect to retinal ganglion cell loss within an age group despite the fact that they are an inbred strain. Some eyes in 15-month-old animals can have near normal RGC counts, similar to those of unaffected mice at 3 months of age.[16] Part of this variability may be related to the variability in IOP among individual eyes[16] or to sex differences. Alternative ways to analyze labeled RGCs can potentially increase our ability to quantify RGC loss beyond measures of total RGC counts.

As illustrated here, automated counting methods may allow for easier extraction of detailed information about RGCs than sampling and manual counting routines. Information that can be obtained from digital images includes not only total RGC counts per retina but also estimates of local density, cell size,

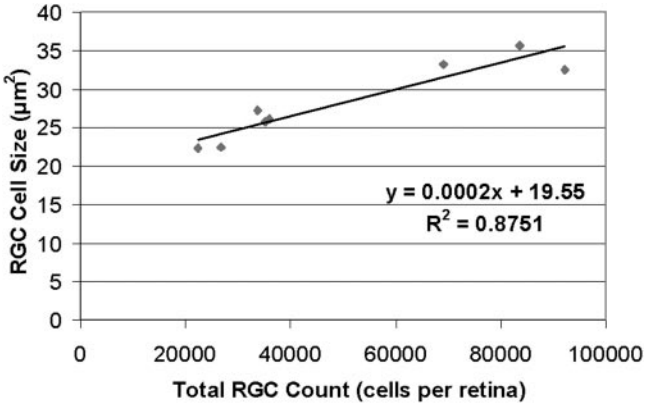

FIGURE 6. Correlation between average RGC cell size and total RGC cell count in senescent DBA/2NNia mice (linear correlation $R^2 = 0.8751$ [$P < 0.001$] for the regression coefficient).

and shape information that allows mapping of RGC loss and survival anywhere in the retina.

NND analysis provides an alternative measure to quantify RGC loss and has the capability to differentiate more uniformly distributed cell loss from the patchy, non-uniform type of loss typical of glaucoma. NND has conceptual homologies to the inverse of the focal cell density calculated for each individual cell and thus does not depend on averaging effects when cells are counted in a representative area (frame) of the retina. As with density, NND defined as centroid-to-centroid distance is affected to some extent by cell size. Despite this limitation, we reasoned that NND might be better able to differentiate between focal and more uniformly distributed RGC loss within each retina, thus providing a better way to model the pattern of RGC loss and allowing comparisons between retinas. Diffuse loss would manifest as a shift of the NND distribution to the right, whereas focal loss would appear as an increase in the proportion of cells with very large NNDs. The NND distribution analysis indicates that both types of loss appear to take place simultaneously in the DBA/2 mouse model of glaucomatous optic neuropathy, suggesting that there may be two pathologic processes leading to RGC depletion in this model of glaucoma. Our findings validate the use of NND as a useful tool for detecting focal and diffuse RGC loss. Examining the effect of the neuroprotective agents/inhibitors of the apoptotic pathway on the distribution characteristics of the NND, as shown in Figure 3, could provide a means to differentiate effects on diffuse or focal RGC loss. Finally, NND analysis can be used to compare different glaucoma models and to provide indications of the type of RGC pathology these models cause in relation to the duration and severity of the insult. An additional important advantage is that NND analysis for a group of retinas provides an overall measure of disease that is less dependent on biologic variability and potential inaccuracies than the single number of a total RGC count derived from manual or automated counting and may prove itself to be more sensitive in detecting early glaucomatous loss. Therefore, the increased statistical power for comparisons of NND distributions may significantly increase our ability to screen for effective treatments that preserve RGCs.

Cell size analysis is an additional capability offered by the construction of digital libraries of all the retrogradely labeled objects (RGCs) within each retina. The large number of RGCs counted by automated methods can overcome shortcomings in accuracy of the absolute cell size compared with more precise estimates derived from a few RGCs in limited areas of the retina captured under high magnification. In the present study, occasional underestimation or overestimation of RGC size because of depth-of-field variations in the captured images or merged cells appears to be random and does not make cell size comparison among retinas any less valid. This conclusion is based on the finding that correlations between cell size and cell loss in the data presented were not affected when the databases were filtered from grossly asymmetric objects representing artifacts or merging of more than one cell (data not shown). The filtering process resulted in the removal of less than 1.5% of the objects and only minimally affected the absolute values of cell sizes and their distribution.

Mean cell size, estimated from the area of the imaged RGCs, in affected retinas of senescent DBA/2 animals appears to be 15% to 20% smaller than in undamaged retinas and results from relative depletion of larger RGCs compared with smaller ones or from cell shrinkage. Larger cells also appear to be located on islands of preserved RGCs within affected retinas. This finding is in agreement with reports that ocular hypertension is associated with an overall size reduction in RGCs in monkey, cat, and rat glaucoma models (Cordeiro MF, et al. *IOVS* 2004;45: ARVO E-Abstract 1114; Guo L, et al. *IOVS* 2004;45:ARVO E-Abstract 2153),[28–32] and has recently been reported to also occur in a rat glaucoma model.[33] The degree of overall cell size reduction in the DBA/2 retina is within the range reported for *Macaca fascicularis* monkeys after 6 to 14 weeks of ocular hypertension.[34] In this study, we present new evidence of spatial correlation between larger cell size and areas of RGC preservation. This result implies the converse, namely that in those areas of a glaucomatous retina in which extensive RGC loss occurs, the largest cells die, or, if they survive, they shrink. Our data, however, could not indicate whether smaller RGCs are less susceptible to injury or whether RGCs in the glaucomatous retina tend to shrink before cell death. Nevertheless our findings show that cell size distribution analysis can provide another measure of the extent of disease in the glaucomatous retina.

In summary, our data confirm the usefulness of automated RGC counting as a method for evaluating glaucomatous retinal damage. Measures of RGC distribution, such as NND, and RGC size can improve our understanding of the pathophysiology of the disease and increase the power of experimental studies. RGC distribution characteristics, such as NND, and RGC cell size complement RGC total cell number as a method of quantifying RGC cell loss in a glaucoma model and offer a more

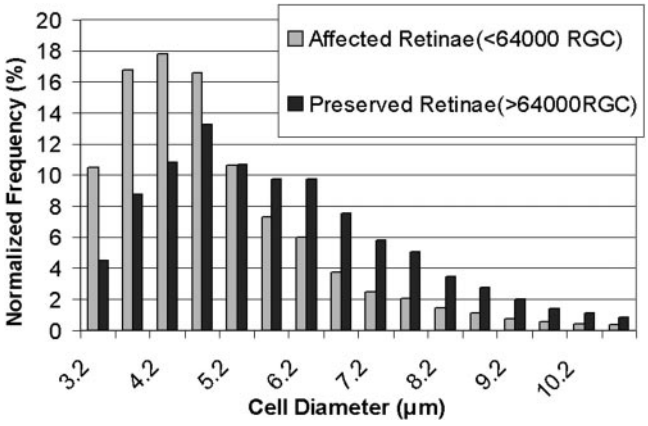

FIGURE 7. Normalized cell size distribution in affected and preserved retinas. The cutoff point for cell counts determined in each retina has been set as 64,000 RGCs—the number of RGCs used for segregating into affected and preserved subgroups—which is 75% of the expected RGC population in young, nonpathologic DBA/NNia retinas. Mean total RGC counts in the preserved group and the affected group are 81,595 cells and 30,856 cells, respectively.

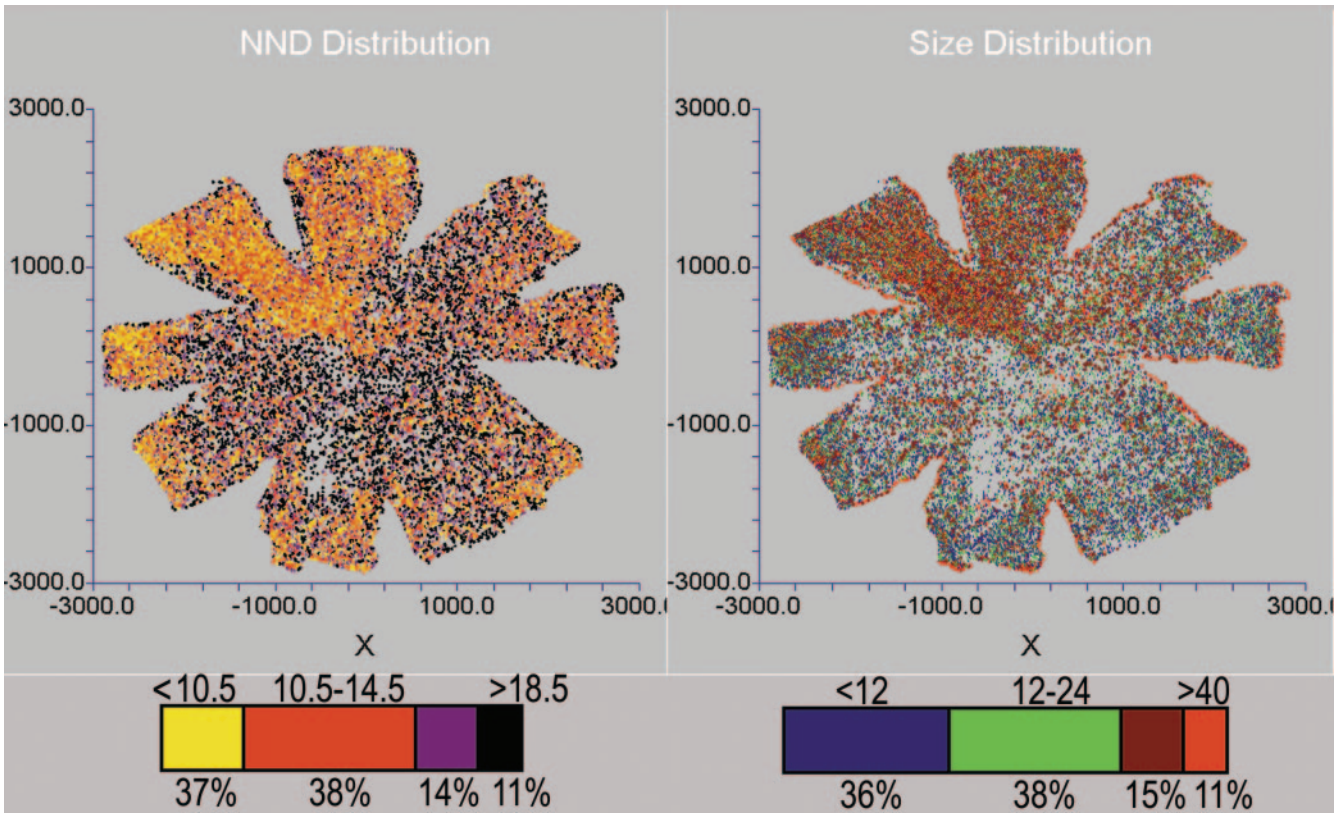

FIGURE 8. NND distribution map (*left*) and object size distribution map (*right*) for one representative retina. The NND distribution map follows the same color-coding scheme seen in Figure 5. Similarly, four bins representing the same proportions of total population as for NND have been chosen for the cell size distribution as well. For size distribution, *brown* data points represent objects (RGCs) with size (cell area) measuring 24 to 40 arbitrary units, and *red* data points represent objects (RGCs) measuring greater than 40 arbitrary units. *Green* and *blue* data points represent RGCs measuring 12 to 24 and less than 12 arbitrary units, respectively (1 arbitrary unit = 1.082 μm^2).

complete description of the disease in the RGC layer. Application of these additional measures of RGC loss may help overcome some of the problems caused by the variability encountered in many glaucoma models.

Acknowledgments

The authors thank Nikolaos K. Robakis (Mount Sinai School of Medicine, New York, NY) for making the Axioskop 2 (Zeiss) available.

References

1. Shareef SR, Garcia-Valenzuela E, Salierno A, et al. Chronic ocular hypertension following episcleral venous occlusion in rats. *Exp Eye Res*. 1995;61:379–382.
2. Vorwerk CK, Lipton SA, Zurakowski D, et al. Chronic low-dose glutamate is toxic to retinal ganglion cells: toxicity blocked by memantine. *Invest Ophthalmol Vis Sci*. 1996;37:1618–1624.
3. Morrison JC, Moore CG, Deppmeier LM, et al. A rat model of chronic pressure-induced optic nerve damage. *Exp Eye Res*. 1997; 64:85–96.
4. Laquis S, Chaudhary P, Sharma SC. The patterns of retinal ganglion cell death in hypertensive eyes. *Brain Res*. 1998;784:100–104.
5. Mittag TW, Danias J, Pohorenec G, et al. Retinal damage after 3 to 4 months of elevated intraocular pressure in a rat glaucoma model. *Invest Ophthalmol Vis Sci*. 2000;41:3451–3459.
6. Neufeld AH, Sawada A, Becker B. Inhibition of nitric-oxide synthase 2 by aminoguanidine provides neuroprotection of retinal ganglion cells in a rat model of chronic glaucoma. *Proc Natl Acad Sci USA*. 1999;96:9944–9948.
7. Gu Z, Yamamoto T, Kawase C, et al. Neuroprotective effect of *N*-methyl-D-aspartate receptor antagonists in an experimental glaucoma model in the rat [in Japanese]. *Nippon Ganka Gakkai Zasshi*. 2000;104:11–16.
8. Wheeler LA, Gil DW, WoldeMussie E. Role of alpha-2 adrenergic receptors in neuroprotection and glaucoma. *Surv Ophthalmol*. 2001;45(suppl 3):S290–S294; discussion S5–S6.
9. Neufeld AH, Das S, Vora S, et al. A prodrug of a selective inhibitor of inducible nitric oxide synthase is neuroprotective in the rat model of glaucoma. *J Glaucoma*. 2002;11:221–225.
10. Huang W, Fileta JB, Dobberfuhl A, et al. Calcineurin cleavage is triggered by elevated intraocular pressure, and calcineurin inhibition blocks retinal ganglion cell death in experimental glaucoma. *Proc Natl Acad Sci USA*. 2005;102:12242–12247.
11. Sheldon WG, Warbritton AR, Bucci TJ, Turturro A. Glaucoma in food-restricted and ad libitum-fed DBA/2NNia mice. *Lab Anim Sci*. 1995;45:508–518.
12. John SW, Smith RS, Savinova OV, et al. Essential iris atrophy, pigment dispersion, and glaucoma in DBA/2J mice. *Invest Ophthalmol Vis Sci*. 1998;39:951–962.
13. Levkovitch-Verbin H, Harris-Cerruti C, Groner Y, et al. RGC death in mice after optic nerve crush injury: oxidative stress and neuroprotection. *Invest Ophthalmol Vis Sci*. 2000;41:4169–4174.
14. Schuettauf F, Quinto K, Naskar R, Zurakowski D. Effects of anti-glaucoma medications on ganglion cell survival: the DBA/2J mouse model. *Vision Res*. 2002;42:2333–2337.
15. Aihara M, Lindsey JD, Weinreb RN. Experimental mouse ocular hypertension: establishment of the model. *Invest Ophthalmol Vis Sci*. 2003;44:4314–4320.
16. Danias J, Lee KC, Zamora MF, et al. Quantitative analysis of retinal ganglion cell (RGC) loss in aging DBA/2NNia glaucomatous mice: comparison with RGC loss in aging C57/BL6 mice. *Invest Ophthalmol Vis Sci*. 2003;44:5151–5162.

17. Chang B, Smith RS, Hawes NL, et al. Interacting loci cause severe iris atrophy and glaucoma in DBA/2J mice. *Nat Genet*. 1999;21: 405–409.
18. Anderson MG, Smith RS, Savinova OV, et al. Genetic modification of glaucoma associated phenotypes between AKXD-28/Ty and DBA/2J mice. *BMC Genet*. 2001;2:1.
19. Aihara M, Lindsey JD, Weinreb RN. Ocular hypertension in mice with a targeted type I collagen mutation. *Invest Ophthalmol Vis Sci*. 2003;44:1581–1585.
20. Bonfanti L, Strettoi E, Chierzi S, et al. Protection of retinal ganglion cells from natural and axotomy-induced cell death in neonatal transgenic mice overexpressing bcl-2. *J Neurosci*. 1996;16:4186–4194.
21. Pennesi ME, Cho JH, Yang Z, et al. BETA2/NeuroD1 null mice: a new model for transcription factor-dependent photoreceptor degeneration. *J Neurosci*. 2003;23:453–461.
22. Danias J, Shen F, Goldblum D, et al. Cytoarchitecture of the retinal ganglion cells in the rat. *Invest Ophthalmol Vis Sci*. 2002;43:587–594.
23. Mo JS, Anderson MG, Gregory M, et al. By altering ocular immune privilege, bone marrow-derived cells pathogenically contribute to DBA/2J pigmentary glaucoma. *J Exp Med*. 2003;197:1335–1344.
24. Russ JC. *The Image Processing Handbook*. 3rd ed. Boca Raton, FL: CRC Press; 1998.
25. Bayer AU, Neuhardt T, May AC, et al. Retinal morphology and ERG response in the DBA/2NNia mouse model of angle-closure glaucoma. *Invest Ophthalmol Vis Sci*. 2001;42:1258–1265.
26. Franklin TR, Druhan JP. The retrograde tracer fluoro-gold interferes with the expression of fos-related antigens. *J Neurosci Methods*. 2000;98:1–8.
27. Paxinos G, Franklin KBJ. The mouse brain in stereotaxic coordinates. San Diego: Academic Press; 2001.
28. Glovinsky Y, Quigley HA, Dunkelberger GR. Retinal ganglion cell loss is size dependent in experimental glaucoma. *Invest Ophthalmol Vis Sci*. 1991;32:484–491.
29. Glovinsky Y, Quigley HA, Pease ME. Foveal ganglion cell loss is size dependent in experimental glaucoma. *Invest Ophthalmol Vis Sci*. 1993;34:395–400.
30. Weber AJ, Kaufman PL, Hubbard WC. Morphology of single ganglion cells in the glaucomatous primate retina. *Invest Ophthalmol Vis Sci*. 1998;39:2304–2320.
31. Shou T, Liu J, Wang W, et al. Differential dendritic shrinkage of alpha and beta retinal ganglion cells in cats with chronic glaucoma. *Invest Ophthalmol Vis Sci*. 2003;44:3005–3010.
32. Cordeiro MF, Guo L, Luong V, et al. Real-time imaging of single nerve cell apoptosis in retinal neurodegeneration. *Proc Natl Acad Sci USA*. 2004;101:13352–13356.
33. Danias J, Shen F, Kavalarakis M, et al. Characterization of retinal damage in the episcleral vein cauterization rat glaucoma model. *Exp Eye Res.* 2006;82:219–228.
34. Morgan JE, Uchida H, Caprioli J. Retinal ganglion cell death in experimental glaucoma. *Br J Ophthalmol*. 2000;84:303–310.